Electroluminescent devices from ionic transition metal complexes

Jason D. Slinker,[a] Jonathan Rivnay,[a] Joshua S. Moskowitz,[a] Jeffrey B. Parker,[a] Stefan Bernhard,[b] Héctor D. Abruña[c] and George G. Malliaras*[a]

Received 19th March 2007, Accepted 22nd May 2007
First published as an Advance Article on the web 6th June 2007
DOI: 10.1039/b704017b

Ionic transition metal complexes (iTMCs) are receiving increased attention as materials capable of yielding efficient electroluminescent devices with air-stable electrodes. The operational characteristics of these devices are dominated by the presence of mobile ions that redistribute under an applied bias and assist in electronic charge injection. This article reviews recent efforts in the field of iTMC devices: i) to understand their physics, ii) to improve their efficiency, colour, turn-on time and lifetime, and iii) to expose their potential applications.

Introduction

Over the past two decades dramatic advances have been achieved in the field of organic electroluminescent devices, which are being developed for display and lighting applications.[1–5] A recent development in this field involves the use of ionic transition metal complexes[5–65] (iTMCs) such as $[Ru(bpy)_3]^{2+}$, where bpy is 2,2′-bipyridine, as shown in Fig. 1. The ionic nature of these materials facilitates the fabrication of efficient devices using air-stable electrodes.[18,36] In addition to efficient operation, the ionic conductivity of iTMCs enables device fabrication by lamination,[38] and the development of simple architectures for large-area illumination panels[39,52] that show fault tolerance and operate directly from a standard outlet.

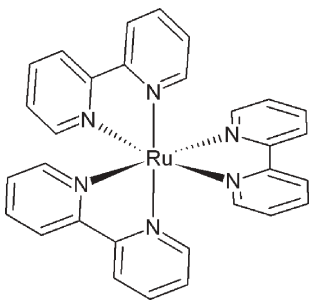

Fig. 1 The structure of $[Ru(bpy)_3]^{2+}$.

In the simplest configuration, an organic light-emitting diode (OLED) consists of a single layer of an organic semiconductor sandwiched between two metal electrodes, the anode and the cathode. Under the application of a bias, holes are injected from the anode into the highest occupied molecular orbital (HOMO) of the organic layer and migrate towards the cathode. In a similar fashion, electrons injected from the cathode into the lowest unoccupied molecular orbital (LUMO) of the organic layer migrate towards the anode. When a hole and an electron meet in the bulk of the organic layer, they may combine to form an exciton. A fraction of these excitons recombine radiatively, giving rise to light emission. The basic requirements from the organic semiconductor are the ability to transport both electrons and holes, and high luminescence efficiency.

[a]*Department of Materials Science and Engineering, Cornell University, Ithaca, New York, 14853-1501, USA. E-mail: ggm1@cornell.edu; Fax: +1 607 255 2365; Tel: +1 607 255 1956*
[b]*Department of Chemistry, Princeton University, Princeton, NY 08544, USA*
[c]*Department of Chemistry and Chemical Biology, Cornell University, Ithaca, New York, 14853-1301, USA*

Jason D. Slinker

Jason Slinker earned his B.S. in Physics, Chemistry and Mathematics from Southern Nazarene University (Bethany, OK, USA) in 2001. He received an M.S. in 2005, and is scheduled to complete a Ph.D. in 2007 in Applied and Engineering Physics from Cornell University. His research with Professor George Malliaras concerns light-emitting devices from ionic transition metal complexes. Jason is currently supported by a National Science Foundation (NSF) Graduate Research Fellowship.

Jonathan Rivnay

Jonathan Rivnay earned his B.S. in Materials Science and Engineering from Cornell University in 2006. He is currently pursuing a doctoral degree in Materials Science and Engineering at Stanford University. His research interests include studies of degradation and structure–property relations of organic semiconductor materials. Jonathan is currently supported by a National Defense Science and Engineering Graduate (NDSEG) Fellowship.

Presently, OLEDs rely upon air-reactive electrodes and multilayer architectures to achieve efficient operation. Air-reactive electrodes come into play as low work function cathodes, which are used to achieve efficient electron injection into the LUMO levels of the adjacent organic layers. Multilayer architectures arise because the emissive materials themselves often do not satisfy the requirements of balanced electronic charge injection and transport. Air-reactive electrodes impose encapsulation requirements on the device, and multilayer architectures often entail multiple evaporation–sublimation steps that require vacuum processing. These requirements increase the cost and time associated with large-scale OLED production.

Ionic transition metal complexes (iTMCs) offer an alternative to such processing associated with conventional OLEDs. In these materials, the complexes themselves support all three processes of charge injection, charge transport, and emissive recombination. Their excellent stability in multiple redox states implies that electronic charges can be readily injected and transported. Furthermore, iTMCs such as $[Ru(bpy)_3]^{2+}(PF_6^-)_2$ are ionically conducting as the PF_6^- counterions can redistribute under an applied bias. This action creates an ionic space charge near each electrode (excess PF_6^- at the anode and uncompensated $[Ru(bpy)_3]^{2+}$ at the cathode), which serves to assist electronic charge injection,[66,67] even to the point of efficiently injecting electrons from air-stable metals.[18,36] In this manner, these devices are similar to the so-called light-emitting electrochemical cells (LECs), which are fabricated by dispersing salts into organic semiconductors.[68] Additionally, the luminescence efficiency of iTMCs can be extremely high, with photoluminescence quantum yields approaching 100%, as emission from these materials arises almost exclusively from triplet states.[3,69–71] As for processing, iTMCs can generally be spin cast directly from solution. These properties indicate that efficient electroluminescent devices can be fabricated from single-layer iTMC devices.

As this follows an earlier review,[5] the previously-described efforts[6–30] in the field will not be discussed in detail, but the significant prior results will be summarized for each section. For additional information on previous work with iTMC devices, we suggest the prior review,[5] the review by Holder *et al.*[3] and that by Coe and Curati.[72] To assist the reader, common ligands used in iTMC devices are depicted in Fig. 2. This review deals only with solid-state devices in which the ionic transition metal complexes were involved in all three processes of charge injection, charge transport and emission—*i.e.* multifunctional chromophores. Along these lines, it should be noted that studies that have concerned blending an iTMC with an electroactive polymer, such as those efforts by Xie *et al.*[73] and Plummer *et al.*,[74] will not be discussed. Neither do we include works where iTMCs were utilized only as luminescent dopants.

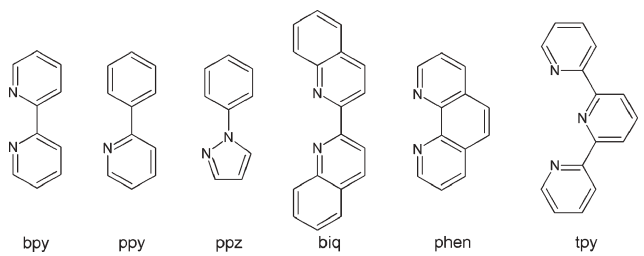

Fig. 2 Common ligands found in ionic transition metal complexes, where bpy is 2,2′-bipyridine, ppy is 2-phenylpyridine, ppz is 1-phenylpyrazolyl, biq is 2,2′-biquinoline, phen is 1,10-phenanthroline, and tpy is terpyridine.

We have divided the review into six sections. The first involves device physics—fundamental experimental and theoretical studies concerning iTMC-device behavior. Next, we will move on to the performance areas of efficiency, colour, lifetime and turn-on time. Finally, we conclude with an outlook section, in which we describe some of the novel architectures and potential applications for iTMC devices.

Device physics

A detailed understanding of iTMC-device operation hinges on studies probing the fundamental mechanisms involved. Of particular importance are experiments that elucidate the processes of electronic charge injection, charge transport, and emission in the device. The following experimental studies provide insight into these processes in iTMC devices.

Providing insight on charge transport of iTMC devices, Chan *et al.*[33] presented results from a series of ionic Ru complexes containing hole-conducting and electron-conducting moieties. Ligands based on 2,2′-bipyridine were symmetrically substituted at the 5,5′ positions or asymmetrically modified with hole-transporting triphenylamine (TPA) and electron-transporting oxadiazole (OXA) units or OXA only. Films were prepared in the inert polymer matrices of polycarbonate or polyvinyl alcohol. Time-of-flight mobilities, μ, of electrons and holes were extracted and both found to be on the order of 10^{-4} cm^2 V^{-1} s^{-1}, with electron mobilities in general being a factor of two higher. The highest mobilities were obtained for complexes having symmetric ligands with both TPA and OXA units. Mobilities were found to be temperature-independent, but exhibited an electric-field (E) dependence such that $\log \mu \sim -E^{1/2}$. This behaviour was attributed to off-diagonal disorder in these materials—the preferred conduction pathways involve hopping steps against the applied field. The complexes having symmetric ligands showed the lowest LUMO gap, associated with the electronic withdrawing nature of the OXA units. Likewise, among the devices based on these films, those with the symmetric TPA and OXA ligands exhibited the best brightness and external quantum efficiencies, suggesting the most balanced bipolar current is achieved in this case.

Rudmann *et al.*[31] investigated $[Ru(bpy)_3]^{2+}$-device performance with complex admittance measurements. The device was modeled as an equivalent circuit of a resistor with a capacitor in parallel. Current–voltage and capacitance–voltage measurements indicated an increase in capacitance at the voltage associated with the onset of current and light emission. This increase was larger for device films with BF_4^- and ClO_4^- counterions *versus* PF_6^-. Transient measurements also revealed that the smaller counterions of BF_4^- and ClO_4^- gave rise to a faster drop in film resistance and increase in capacitance upon DC driving than did PF_6^-. These results

were interpreted within the framework of an electrochemical model, and parameters concerning electrochemical junction formation were extracted. By assuming a parallel-plate capacitor model, it was determined that for devices with an iTMC layer approximately 120 nm thick, the electrochemical junction formed was approximately 60 nm thick for devices with BF_4^- and ClO_4^- counterions, and 10 nm thicker for devices with PF_6^- counterions. Numerical modeling based upon the Nernst equation and Ohm's law predicted that a large electric field forms in the center of the device rather than at the electrodes, contrary to the modeling results of deMello *et al.*[66,67]

The effects of various top and bottom electrodes on $[Ru(bpy)_3]^{2+}(PF_6^-)_2$-device performance were studied by Gorodetsky *et al.*,[36] with results shown in Fig. 3. Top electrodes were composed of gold, silver or aluminium layers, and bottom contacts were either indium–tin oxide (ITO) or Pt-coated ITO. Under forward bias, with the bottom electrode wired as the anode, the steady-state device characteristics were independent of the electrodes used. For devices having an ITO anode, cathodes of Al, Ag, and Au gave identical currents and radiant fluxes, taking into account the differences in reflectivities of the electrodes. For devices with Au top contacts, coating the ITO with a thin layer of Pt also did not affect the steady-state current or radiant flux. These results were interpreted as a consequence of the ionic space-charge effects—the PF_6^- ions redistribute in each case to effectively inject both holes and electrons. However, this was not the case under reverse bias. For Al and Ag top contacts, the radiant flux decayed rapidly, corresponding to electrochemical breakdown of these electrodes. For a device having a Au top contact and a Pt-modified bottom electrode, reversed-bias operation yielded slower turn-on times than those with bare ITO electrodes, as the Pt electrode has a higher work function and therefore required more PF_6^- ions to effectively inject electrons. This work demonstrated that, for $[Ru(bpy)_3]^{2+}(PF_6^-)_2$, air-stable electrodes are sufficient for efficient device operation. However, this is not always the case with iTMC devices. For instance, several Ir complexes have shown differences in device operation with different top contacts, requiring lower work function electrodes for efficient operation in some cases.[26,40,46] In these systems, the bandgap is larger and the ionic conductivity is lower, factors that likely preclude sufficient counterion redistribution to inject electrons efficiently in all cases.

The temperature dependence of the current, radiant flux and efficiency of $[Ru(bpy)_3]^{2+}(PF_6^-)_2$ devices was explored by Slinker *et al.*[37] over the temperature range 200–380 K. The

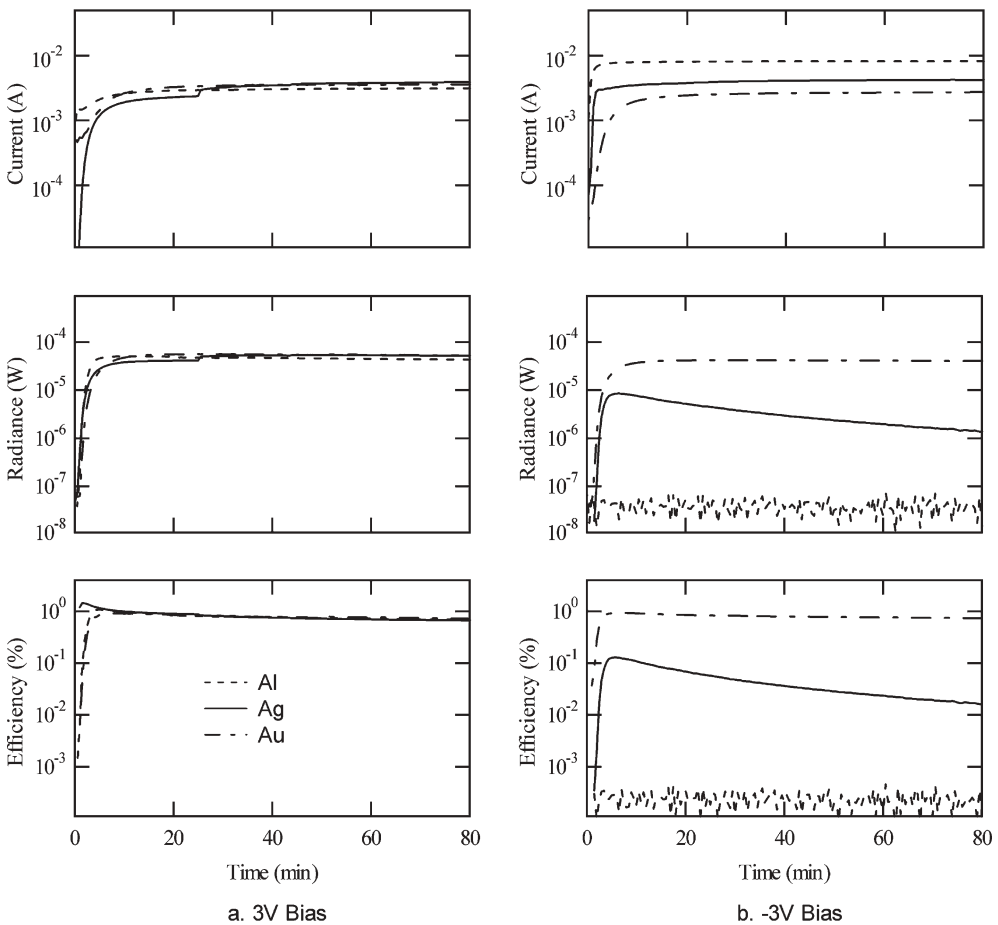

Fig. 3 (From Fig. 1, ref. 36.) Temporal evolution of the current, radiance and efficiency of ITO/$[Ru(bpy)_3]^{2+}(PF_6^-)_2$/M devices under forward (a) and reverse (b) bias. M stands for Al, Ag, or Au. Reproduced with permission from *Appl. Phys. Lett.*, 2004, **84**, 807–809. Copyright 2004, American Institute of Physics.

current was found to exhibit Arrhenius-type behavior, increasing monotonically with temperature, with distinct low-temperature and high-temperature regimes. For 2.4 V operation, the radiant flux was found to reach a maximum at approximately 315 K. The temperature dependence of the external quantum efficiency was elucidated with *in situ* photoluminescence (PL) measurements, with PL being measured directly from the device in operation. It was found that the temperature dependence of the external quantum efficiency followed that of the PL quantum yield, implying that the recombination efficiency did not change with temperature and that the contacts were ohmic throughout the 200–380 K temperature range at 2.4 V. Both the external quantum efficiency and PL quantum yield showed a monotonic decrease with temperature. This quenching was attributed to thermal activation of electrons to a d orbital that results in non-radiative d–d transitions to the ground state. Furthermore, luminescence quenching was shown to be distinctively enhanced upon electrical driving.

Efficiency

External quantum efficiency (EQE), the ratio of photons emerging from the device per electron injected, is a critical figure of merit for evaluating device performance. Related to this figure are the power efficiency, usually reported as emitted flux in lumens per electrical Watt (Lm W^{-1}), and the current efficiency, usually cited as emitted flux in candelas per electrical ampere (cd A^{-1}). Obviously, these terms are crucial in the evaluation of iTMCs for display and solid-state lighting applications. The following observations and trends were noted in our previous review:

• High EQE can be realized from devices based on a single layer of an iTMC between two electrodes.[14,16,18,26]

• EQE is found to increase by mixing the complex with an inert polymer, such as poly(methyl methacrylate) (PMMA) or poly(carbonate) (PC).[17,20] This increase is likely due to a decrease in self-quenching that occurs when complexes are in close proximity with one another (however, this technique typically imposes a corresponding drop of power efficiency due in part to increased resistance of the film).

• Bulky side chains on the ligands of the complex can lead to an improved EQE for the same reason.[24,26]

• The morphology of the iTMC layer can be manipulated to increase EQE, such as by making crystalline films.[19]

• Iridium, osmium, and other third-row transition metal complexes offer the possibility of greater EQE due to an increased ligand-field splitting energy, which inhibits non-luminescent pathways of electron-hole recombination.[18,26]

Subsequent efforts have produced substantial advances in raising the maximum external quantum efficiency of iTMCs. Some efforts involve evaluating new compounds, such as novel iridium and copper complexes. Other efforts have sought to suppress luminescence-quenching mechanisms of existing materials. A plot of the evolution of the maximum reported quantum efficiency with time is shown in Fig. 4.

Liu and Bard[35] showed that zone annealing improved the efficiency of $[Ru(bpy)_3]^{2+}(ClO_4^-)_2$ devices. Thin films were annealed by slowly passing a hot wire across the freshly

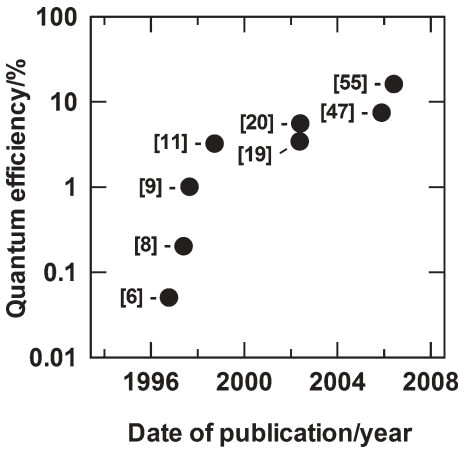

Fig. 4 Evolution of the record external quantum efficiency with time. The corresponding reference is given for each data point.

spin-coated iTMC film, enhancing the conversion of the amorphous complex layer to a film having large crystal domains. Resulting devices had EQEs up to 3.6%, about a factor of 2 greater than values previously reported for devices that were prepared in a conventional vacuum oven. This increase correlated with an increase in improved photoluminescence efficiency upon zone annealing.

A multilayer structure was shown by Liu and Bard[42] to improve the efficiency of $[Ru(bpy)_3]^{2+}(ClO_4^-)_2$ devices. Devices were fabricated in the structure ITO/Alq_3/$[Ru(bpy)_3]^{2+}(ClO_4^-)_2$/Ga–In, where the aluminium 8-hydroxyquinoline (Alq_3) layer served as a hole-transport layer and an electron-blocking layer. A maximum EQE and power efficiency of 6.4% and 5.3%, respectively, were attained, with emission occurring entirely within the $[Ru(bpy)_3]^{2+}(ClO_4^-)_2$ layer. Such efficiency values are considerably higher than those reported for single-layer $[Ru(bpy)_3]^{2+}(ClO_4^-)_2$ devices. This enhancement was ascribed to a shift in the recombination zone from the ITO electrode to the center of the device by inclusion of the Alq_3 layer, thus limiting exciton quenching at the electrodes.[28]

Highly efficient devices covering a significant portion of the visible spectrum were reported by Tamayo *et al.*[47] Using Ir complexes with the base structure $[Ir(ppz)_2(bpy)]^+$ or $[Ir(ppz)_2(biq)]^+$, where ppz is 1-phenylpyrazolyl and biq is 2,2′-biquinoline, devices with external quantum efficiencies of up to 7.4% and power efficiencies up to 25 Lm/W were realised. These devices are described in further detail in the colour section.

Likewise, highly efficient iridium complexes were realised by Su *et al.*[65] In particular, the orange-emitting $[Ir(ppy)_2(SB)]^+(PF_6^-)$ (shown in Table 1) and green-emitting $[Ir(dFppy)_2(SB)]^+(PF_6^-)$ complexes were reported, where SB is 4,5-diaza-9,9′-spirobifluorene and dFppy is 2-(2,4-difluorophenyl)pyridine. The bulky SB ligand was selected to provide steric hindrance and reduce self-quenching. Photoluminescence (PL) quantum-yield measurements of neat films gave comparable values to those blended in an apolar host, indicating that the ligands themselves inhibited non-radiative pathways associated with self-quenching. This was reflected both in the EQEs, which were as high as 7.1% for

Table 1 Structure and electroluminescent properties of selected iridium complexes

Name	$[Ir(F\text{-}mppy)_2(dtb\text{-}bpy)]^+(PF_6^-)$	$[Ir(dF\text{-}ppz)_2(dtb\text{-}bpy)]^+(PF_6^-)$	$[Ir(ppy)_2(SB)]^+(PF_6^-)$	$[Ir(ppy\text{-}Pbu_3)_3]^{3+}(PF_6^-)_3$ (w/20% PMMA)
Structure	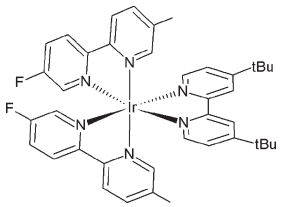	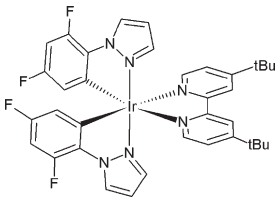	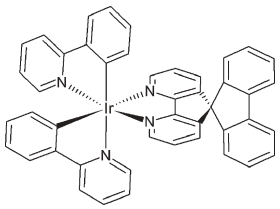	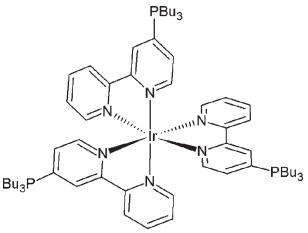
λ_{max}	542	492	585	487
CIE	0.37, 0.58	0.20, 0.41	n/a	0.34, 0.50
Ref.	40	47	65	44

[a] *t*Bu and Bu are *tert*-butyl and *n*-butyl groups, respectively

each complex, and the power efficiencies, which were 22.6 and 26.1 Lm W^{-1} for the unmodified and fluoro-modified compounds, respectively. The results of Tamayo *et al.*[47] and Su *et al.*[62] reveal that iridium iTMC devices can yield efficiencies comparable to those based on neutral complexes.

The effects of dispersing one iTMC complex into another were observed by two groups. An ionic osmium complex, $[Os(phen)_3]^{2+}(PF_6^-)_2$ (phen = 1,10-phenanthroline), was doped by Hosseini *et al.*[48] at various concentrations into a $[Ru(bpy)_3]^{2+}(PF_6^-)_2$ matrix. Even though the pristine Os complex device was substantially less efficient than the pristine Ru device, a blended device containing 5% w/w Os complex in the Ru matrix exhibited a higher EQE than either pristine device, with emission arising almost entirely from the Os complex. This improvement indicated a decrease in self quenching of $[Os(phen)_3]^{2+}(PF_6^-)_2$ emitters upon dispersion in the matrix. Su *et al.*[62] extended this concept to Ir complexes by doping the green-emitting $[Ir(dFppy)_2(SB)]^+(PF_6^-)$ complex with the orange-emitting $[Ir(ppy)_2(SB)]^+(PF_6^-)$ complex described above. The highest PL quantum yield was obtained for films with guest concentrations of 25% w/w, at which concentration emission was found to almost completely occur from the guest. An impressive peak EQE of 10.4% and power efficiency of 36.8 Lm W^{-1} were obtained. As in the previous case, the improvement in efficiency over either pristine film signified a decrease in self-quenching of emission upon doping in a matrix.

Reporting the highest efficiencies to date for iTMC devices, Zhang *et al.*[55] investigated the copper complex [Cu(dnbp)(DPEphos)]$^+(BF_4^-)$, where the ligand dnbp is 2,9-di-*n*-butyl-1,10-phenanthroline and DPEphos is bis[2-(diphenylphosphino)phenyl]ether, as shown in Table 2. Single-layer devices based on thin films of this material yielded current efficiencies as high as 56 cd A^{-1} at 10 cd m^{-2} and 53 cd A^{-1} at 100 cd m^{-2}, the former value corresponding to an EQE of 16%. These values were obtained upon pre-biasing a device for 40 s at 25 V, then reducing the bias to a lower value, following the technique first suggested by Handy *et al.*[14] A power efficiency of 42 cd A^{-1} was obtained upon pure DC driving of the device at 10 V. Efficiencies were independent of the choice of electrodes used (ITO/Cu complex/M, where M is Ag, Al or Ca). These high efficiencies were attributed to steric hindrance of excited-state relaxation to nonradiative pathways by the bulky ligands of the Cu complex. These results suggest that it is possible to achieve very high EQE from a single-layer, solution-processable device.

Table 2 Structure and electroluminescent properties of selected ruthenium and copper complexes

Name	$[Ru(bpy)_3]^{2+}(PF_6^-)_2$	$[Ru(tpy)(tpy\text{-}CO_2Et)]^{2+}(PF_6^-)_2$	$[Cu(dnbp)(DPEphos)]^+(BF_4^-)$	$[Cu_2(tdpme)_2(4,4'\text{-}bpy)]^{2+}(BF_4^-)_2$ (w/PEO)
Complex structure	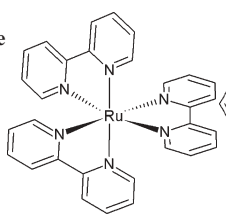	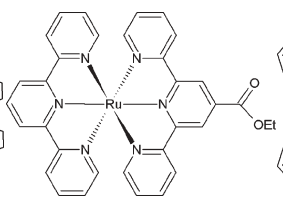	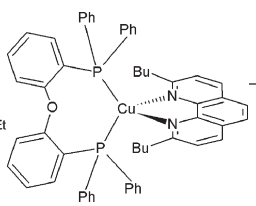	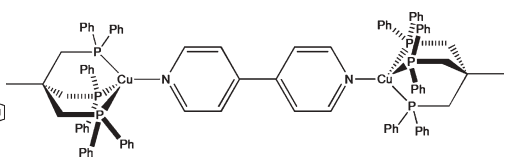
λ_{max}	609	706	523 540 (w/25% PMMA)	590 (+12 V) 618 (−12 V)
CIE	0.62, 0.37	0.72, 0.28	0.25, 0.60	0.57, 0.42 (+12 V)
Ref.	5	44	55	49

[a] Et, Bu and Ph are ethyl, *n*-butyl, and phenyl groups, respectively.

Similarly, Armaroli *et al.*[54] fabricated an LEC from the same copper complex mixed with poly(methyl methacrylate) (PMMA) to produce a film with 25% polymer (w/w). PMMA, as noted, was used to enhance the film-forming capabilities and decrease self-quenching.[17,20] Single-layer devices were prepared in the configuration ITO/{[Cu(dnbp)(DPEphos)]$^{+}$(BF_4^-) + PMMA}/Ag; however, these devices showed a significantly lower efficiency of 0.5–1 cd A^{-1}. This lower result is in conflict with the result of Zhang *et al.*,[55] who claim results of two orders of magnitude higher efficiency for similarly prepared-devices.

Obviously, there is still a need for higher efficiencies in these devices. Although there are several complexes with high photoluminescence efficiencies in solution, these do not necessary result in high efficiency devices. Further understanding and minimization of self-quenching represents a promising strategy. In addition, energy transfer from an iTMC host to efficient emitters needs to be fully explored. Charge balance is usually achieved in devices that utilize iTMCs with a small bandgap, but it is not necessarily attained in devices using high bandgap complexes. Therefore, careful optimization of charge balance is important in screening of new materials.

Colour

As with any materials class targeted for lighting and/or display applications, tuning of the colour to achieve red, green, and blue emission is a particularly important feature, as mixing these colours produces any colour in the spectrum, including white. One often-used metric is the peak wavelength of the electroluminescence spectrum, noted λ_{max}. Also, the Commission Internationale de l'Eclairage (CIE) coordinates provide the colour purity relative to the red, green and blue receptors of the human eye.

During their early development, little work focused on colour tuning of iTMC-based devices. With the main focus on efficiency, the vast majority of devices utilized ruthenium and osmium-based complexes, which typically emit in the red and orange–red part of the spectrum. Only recently has extensive research been conducted to produce additional colours. Previous observations concerning colour tuning were:

• Ester-substituted ligands were found to red-shift the emission of $[Ru(bpy)_3]^{2+}(PF_6^-)_2$.[14,16]

• The iridium complex $[Ir(ppy)_2(dtb\text{-}bpy)]^{+}(PF_6^-)$, where dtb-bpy is 4,4′-di-*tert*-butylbipyridine, was found to produce yellow emission (λ_{max} = 560 nm) under forward bias.[26] Iridium was shown to have promise for colour tuning over ruthenium complexes due to increased ligand-field splitting energies. Because the vacant π*-orbitals in iridium(III) complexes are localized on the ligands, deliberate chemical synthesis can be used to tune emission. The majority of subsequent iTMC colour tuning has centered on appropriate selection of ligand chemistry or transition metal core.

Terpyridyl ruthenium(II) complexes have received recent attention as materials capable of deep red emission. Ng *et al.*[32] reported a series of polyimides containing a terpyridyl Ru complex on the main chain. Device electroluminescence showed deep-red emission centered at about 650 nm and near infrared (IR) emission centered near 750–800 nm. The red emission was designated a π*(tpy) → d(Ru) transition, while the IR emission was believed to arise from the imide component. EQEs and luminances of up to 0.1% and 120 cd m^{-2} were attained, apparently bolstered by the polymer matrix. Promising photovoltaic properties were also observed. Likewise, Bolink *et al.*[44] have achieved a deep red emission using the small-molecule bis-chelated Ru complex $[Ru(tpy)(tpy\text{-}CO_2Et)]^{2+}(PF_6^-)_2$, as shown in Table 2. The ester substituents were found to significantly improve the quantum efficiency over the unsubstituted terpyridyl complex. These devices showed lower brightness (<10 cd m^{-2}) and external quantum efficiency. Both of these efforts are noteworthy, however, as low efficiency is a general phenomenon of terpyridyl Ru complexes. This is because the luminescent ^{3}MLCT state is quenched by low lying ^{3}MC levels due to poor bite angles of the tpy ligands.[75] Hence, the mere observation of measurable electroluminescence in terpyridyl Ru devices is significant.

Continuing work with ionic iridium complexes, green emission[40] was first achieved in an iTMC device with the Ir complex $[Ir(F\text{-}mppy)_2(dtb\text{-}bpy)]^{+}(PF_6^-)$, which is depicted in Table 1. The fluorine substituents on the phenylpyridine ligands caused a blue shift of the emission spectrum relative to similar, unfluorinated complexes. This colour shift, relative to $[Ir(ppy)_2(dtb\text{-}bpy)]^{+}(PF_6^-)$, was attributed to strong inductive and mesomeric effects of the fluoro substituent on the phenyl ring of the 2-phenylpyridyl ligand. The pristine device showed a maximum external quantum efficiency of 1.8% and emission at λ_{max} = 542 nm, a figure that was independent of the bias direction and electrodes used. However, addition of an ionic liquid to the iTMC layer to improve turn-on time (as discussed below) introduced a bias-dependent shift in the electroluminescence spectrum (531 nm at +3 V, 558 nm at −3 V).

Utilizing a heavily fluorinated iTMC, Lowry *et al.*[46] fabricated devices with blue–green emission. Using an Ir complex with two multifluorinated cyclometalating ppy ligands, $[Ir(dF(CF_3)ppy)_2(dtb\text{-}bpy)]^{+}(PF_6^-)$, where (dF(CF$_3$)ppy) is 2-(2,4-difluorophenyl)-5-trifluoromethylpyridine, an emission of λ_{max} = 500 nm was achieved (CIE = 0.20, 0.51). Interestingly, as seen in $[Ir(ppy)_2(dtb\text{-}bpy)]^{+}(PF_6^-)$,[26] a blue shift in emission from 520 nm to 500 nm occurred from positive to negative voltages. A maximum EQE of 0.75% was obtained. To understand the origin of the colour tuning, the energy levels of a series of $[Ir(ppy)_2(dtb\text{-}bpy)]^{+}$ complexes with increasing fluorine content were probed electrochemically and modeled by density functional theory (DFT). It was concluded that the metal-centered HOMO level is highly stabilized by introduction of the fluorine atoms.

Tamayo *et al.*[47] demonstrated the ability to tune the emission colour across a substantial portion of the visible part of the spectrum by varying the electrochemical gap of the parent compound $[Ir(ppz)_2(bpy)]^{+}(PF_6^-)$, where ppz = 1-phenylpyrazolyl. They demonstrated that independent tuning of the HOMO and LUMO levels is possible though substitution of the cyclometalate or the diimine, respectively. Green emission (λ_{max} = 542 nm; CIE = 0.37, 0.59) is observed from the compound $[Ir(ppz)_2(dtb\text{-}bpy)]^{+}(PF_6^-)$, which operated at a peak EQE of 6.9% with a corresponding luminance of

11 500 cd m^{-2}. Blue green emission (λ_{max} = 492 nm) was achieved by substituting the 4′ and 6′ positions on the ppz ligand with electron-withdrawing F atoms ($[Ir(dF\text{-}ppz)_2(dtb\text{-}bpy)]^+(PF_6^-)$, shown in Table 1). Red emission (λ_{max} = 635 nm; CIE = 0.67, 0.32) was achieved by changing the diimine ligand from bpy to 2,2′-biquinolyl (biq) and making $[Ir(tb\text{-}ppz)_2(biq)]^+(PF_6^-)$, where tb = 5′-*tert*-butyl. The blue green and red emitting compounds had EQEs of 4.6% and 7.4%, and brightness of 1700 cd m^{-2} and 7500 cd m^{-2}, respectively. LECs based on these complexes exhibited long turn-on times of ~30 min to reach 1 cd m^{-2}. No voltage dependence on EL spectra was observed. The spectra from these devices are presented in Fig. 5.

Nazeeruddin *et al.*[60] similarly achieved blue green emission from a single-layer Ir complex LEC by varying the ligand chemistry. In this case, the colour tuning was achieved by destabilization of the LUMO rather than stabilization of the HOMO. Under a 5 V bias, a blue–green EL emission ($\lambda_{max} \approx$ 520 nm) and a maximum EQE of 0.2% is observed from a $[Ir(ppy)_2(dma\text{-}bpy)]^+(PF_6^-)$ device, where dma-bpy is 4,4′-(dimethylamino)-2,2′-bipyridine. Through electrochemistry it was revealed that the introduction of the electron-donating dimethylamino groups significantly destabilizes the LUMO relative to the HOMO when compared to $[Ir(ppy)_2(dtb\text{-}bpy)]^+(PF_6^-)$, resulting in blue-shifted emission.

Likewise, colour tuning of Ir complexes was done by Su *et al.*[65] Emission was shifted from orange (λ_{max} = 585 nm) for $[Ir(ppy)_2(SB)]^+(PF_6^-)$, shown in Table 1, to green (λ_{max} = 530 nm) for $[Ir(dFppy)_2(SB)]^+(PF_6^-)$ through introduction of fluoro groups on the ppy ligand.[40,46] In addition, using the SB ligand over the dtb-bpy ligand red shifted the emission.

Bolink *et al.*[51] used a different approach to tuning Ir complexes—attaching a charged side group on the periphery of the cyclometalating ligands. By adding phosphonium groups to ppy ligands, the authors converted an otherwise neutral complex into an iTMC. A blue–green emission (λ_{max} = 487 nm) and a maximum power efficiency of 1.4 cd A^{-1} were observed for $[Ir(ppy\text{-}Pbu_3)_3]^{3+}(PF_6^-)_3$ (shown in Table 1)

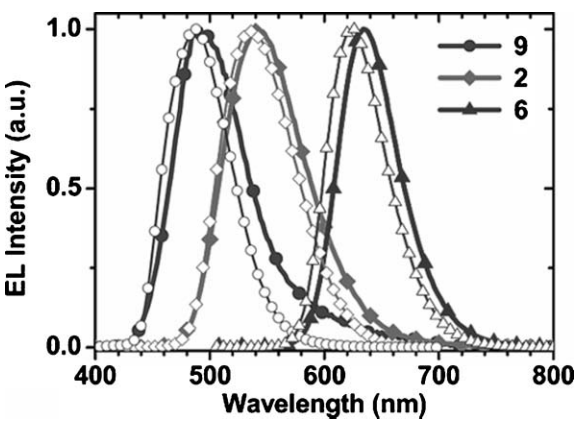

Fig. 5 (From Ref. 47, Fig. 7) Electroluminescence (EL, solid symbols) and photoluminescence (PL, open symbols) spectra from three Ir complexes. Compound **9** is $[Ir(dF\text{-}ppz)_2(dtb\text{-}bpy)]^+(PF_6^-)$, compound **2** is $[Ir(ppz)_2(dtb\text{-}bpy)]^+(PF_6^-)$, and compound **6** is $[Ir(tb\text{-}ppz)_2(biq)]^+(PF_6^-)$. Reproduced with permission from *Inorg. Chem.*, 2005, **44**, 8723–8732. Copyright 2005, American Chemical Society.

blended with 20% PMMA. This blue shift, compared to the $Ir(ppy)_3$ complex, was attributed to the electron-withdrawing nature of the tri-butyl phosphorous group on the phenyl-pyridine ligand. The observed blue–green emission was found to shift to λ_{max} = 570 nm after 100 s of operation at 4 V.

Some groups have found EL spectral shifts in devices upon bias magnitude or direction,[26,46] and Wang *et al.*[49] suggest a mechanism for such a phenomenon. With a dinuclear copper iTMC, $[Cu_2(tdpme)_2(4,4'\text{-}bpy)]^{2+}(BF_4^-)_2$ (as shown in Table 2), blended with PEO to form the active layer, they showed a red shift in EL to λ_{max} = 590 nm at +12 V compared to the PL spectra (λ_{max} = 555 nm). In reverse bias, a further red shift was observed, to λ_{max} = 618 nm (−12 V). Based on electric field theory and the LEC device mechanism, they suggest that such a shift is due to the polarization effect of molecular orbitals under the high electric fields in the device.

As noted above, copper-based complexes have been employed as LEC-active layers, and cases of green emission have been disclosed. Armaroli *et al.*[54] noted that the $[Cu(dnbp)(DPEphos)]^+(BF_4^-)$ complex, depicted in Table 2, yielded electroluminescence at $\lambda_{max} \approx$ 540 nm. Similarly, Zhang *et al.*[55] found highly efficient (56 cd A^{-1}, 16% EQE) operation from the same copper complex. In this case, green EL with λ_{max} = 523 nm was reported for single-layer complex films.

While there has been much effort in tuning colour through iTMC chemistry, some work has dealt with fine tuning of colour using dopants. Hosseini *et al.*[48] showed that the addition of a phosphorescent dopant into an iTMC matrix allows for fine tuning of EL spectra. By varying the concentration of the $[Os(phen)_3]^{2+}(PF_6^-)_2$ dopant in a $[Ru(bpy)_3]^{2+}(PF_6^-)_2$ matrix from 1 to 5% w/w, fine-tuned emission from 610 to 710 nm was demonstrated. At 5% doping, nearly all the emission was attributed to the Os dopant (λ_{max} = 695 nm). Additionally, the emission showed a voltage dependence at lower dopant concentrations. At higher bias, emission from the $[Ru(bpy)_3]^{2+}$ matrix was more pronounced, while that from the Os dopant was independent of bias. This was attributed to saturation of the dopant excited-states.

Similarly, deep red and near infrared (IR) emission was evoked by Gong *et al.*[34] by blending a $[Ru(bpy)_3]^{2+}(PF_6^-)_2$ complex with CdS nanoparticles. The bpy ligands of the Ru complex were modified with oxidiazole (OXA) and triphenyl-amine (TPA) moieties.[12,33] Devices based on polyvinyl alcohol–Ru complex–CdS blends showed enhanced emission in the 700–800 nm range *versus* those with no nanoparticles, for which emission was centered about 650 nm. It was also observed that the maximum EQE and lifetime were also increased upon addition of the nanoparticles.

Infrared emission has also been obtained from iTMCs by Wang *et al.*,[59] who obtained IR electroluminescence as deep as λ_{max} = 790 nm. The emissive materials were co-polymers, with one monomer containing pendant dinuclear ruthenium groups and the other 4-vinylbenzoate. The best EL performance was found for the polymer prepared with the highest ruthenium content (1 : 3.2 ruthenium-to-benzoate monomer molar ratio). The EL, observed at λ_{max} = 790 nm, coincided with the PL and was attributed to the ^{3}MLCT state, as in other dinuclear ruthenium complexes. The maximum EQE was approximately

5×10^{-4}%. Nevertheless, this preliminary work demonstrates that iTMCs may have utility as infrared emitters.

A number of groups have also investigated incorporating iTMCs into multilayered OLED structures. Voltage-controlled colour tuning has been achieved by Zhen *et al.*[45] and Wang *et al.*,[58] using a hybrid OLED/LEC multilayered cell. By introducing a 30 nm spun-cast $[Ru(bpy)_3]^{2+}(PF_6^-)_2$ layer on ITO and vapor depositing additional well-known OLED layers on top, a voltage-controlled cell was attained. Two examples from Wang *et al.*[58] include a green–red variable cell (using Alq_3 as the active green emitter, λ_{max} = 530 nm), and blue-red variable cell (using 4,4′-bis(2,2′-diphenylvinyl)-1,1′-biphenyl DPVBi as the active blue emitter, $\lambda_{max} \approx$ 450 nm). In both cases the Ru-complex layer emitted at λ_{max} = 620 nm and dominated at high voltages (18–20 V), while the traditional OLED active material dominated at lower voltages ($\approx$ 8 V). Thus, there coexisted two emitting areas, one based on traditional organic LED contributions from the Alq_3 or DPVBi layer and the other based on the Ru iTMC complex layer. In the case of Zhen *et al.*,[45] their multilayer device showed polarity-dependent emission, with complex-only emission under reverse bias and mixed contributions under forward bias. In all cases, the applied bias can change the contributing proportions of each component, and hence the overall colour of emission.

The preceding efforts mark significant advances in extending the colour gamut of iTMC devices. Though some studies into the blue portion of the spectrum have been reported, saturated and stable blue emission still remains a challenging target. Blue emission is required for full-colour displays and illumination-quality white light.

Lifetime

Lifetime is an important figure-of-merit when evaluating the durability of devices for display or lighting applications. Lifetime is often quantified by the half-life $t_{1/2}$, the time for the radiant flux to decay to ½ of its maximum value. Previous observations concerning lifetime of iTMC devices include:

- Higher voltages tend to decrease lifetime.[7,8,14,24]
- Blending an iTMC in an inert polymer can improve lifetime, yielding a $t_{1/2}$ as high as 1000 h.[17,20]
- The choice of metal contacts was found to influence the lifetime, even for devices stored in the off state.[17,22] For example, devices with Ag contacts were found to yield superior stability over those with Al.
- Crystalline films showed improved lifetimes over amorphous films.[19]
- Smaller counterions can lead to lower device-lifetimes.[20]
- $[Ru(bpy)_3]^{2+}$-device degradation involves the formation of a photoluminescence quencher, perhaps in small quantities on the order of 1% w/w.[24,27] One suggested quencher was the complex $[Ru(bpy)_2(H_2O)_2]^{2+}$.[27]

Determined by factors such as chemical reaction of the complexes and electrochemical reactions at the electrodes, lifetime is highly environmentally-specific. Furthermore, for DC driving, the current of the device evolves with time, which can contribute to complex shapes of radiant flux *versus* time curves, obscuring the meaning of $t_{1/2}$. Finally, in general, running devices at a higher luminance leads to lower lifetimes, so high lifetime can often be claimed at the expense of luminance. All of these factors complicate comparing lifetimes across different groups. Therefore, we will provide an extended example to illustrate some of these issues and provide an alternative method to understand device stability.

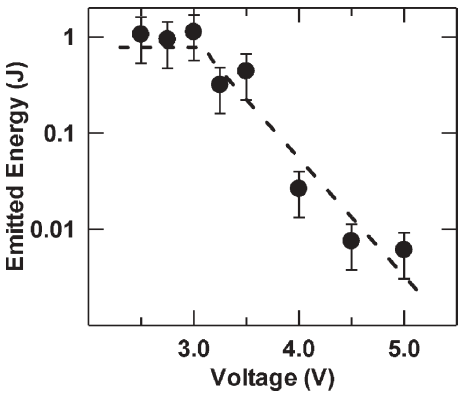

Fig. 6 Total emitted energy E_{tot} *versus* bias for an ITO/$[Ru(bpy)_3]^{2+}(PF_6^-)_2$/Au device.

A convenient way to analyze degradation of electroluminescent devices was introduced by Kalyuzhny *et al.*[27] Rather than simply reporting a decay time of the radiant flux itself, one records the integral of the radiant flux *versus* time curve—the total emitted energy, E_{tot}.[27,41] E_{tot} provides a good measure for comparing different materials, as it takes into account the absolute magnitude of the radiant flux as well as the total device lifetime, and it does not rely on the shape of the radiant flux *versus* time curve. Furthermore, E_{tot} represents the total number of photons emitted from the device over its lifetime. This factor is physically significant, as degradation of iTMCs involves the formation of a quencher upon passage of bipolar current.[27] A device more resistant to this degradation process would presumably be one that yields a higher E_{tot}.

The conventional method[27,41] for calculating E_{tot} from a device is to integrate the radiant flux *versus* time curve from t = 0 (application of bias) to $t = t_{1/5}$, where $t_{1/5}$ is the time for the total radiant flux to decay to ⅕ of maximum (the factor $t_{1/5}$ is an alternative measure of lifetime and analogous to $t_{1/2}$). If this value is divided by the electrode area, giving a total emitted energy-density U_{tot}, then one can compare electrodes of arbitrary shapes. In the following examples, electrode area is held at a constant value of 3 mm^2, so we will restrict our discussion to the more intuitive quantity of E_{tot}.

An example of E_{tot} plotted against the applied bias for ITO/$[Ru(bpy)_3]^{2+}(PF_6^-)_2$/Au devices is given in Fig. 6.† The error bars were derived from the variance of several $[Ru(bpy)_3]^{2+}(PF_6^-)_2$ devices operated at 3 V. Two regimes are evident in this plot. The first one is for voltages lower than 3.2 V, where E_{tot} is independent of bias, in good agreement

† ITO/$[Ru(bpy)_3]^{2+}(PF_6^-)_2$/Au devices were fabricated from an acetonitrile solution containing 40 mg complex per mL. Likewise, devices with PMMA were fabricated by blending the above solution 1 : 1 with an acetonitrile solution containing 25 mg of PMMA per mL. Films were baked for 2 h at 120 °C under nitrogen atmosphere and were never exposed to air. Preparation of the complex and details on the device testing are as described in Ref. 24.

with the report by Kalyuzhny *et al.*[27] The second regime is for voltages higher than 3.2 V, where E_{tot} drops dramatically with bias.

In the first regime, the average radiant flux R of a device is inversely proportional to its lifetime as E_{tot} = constant = $Rt_{1/5}$. For the $[Ru(bpy)_3]^{2+}(PF_6^-)_2$ example, if E_{tot} = 1 J, a 3 mm^2 device operating at 200 cd m^{-2} would yield a $t_{1/5}$ of 35 hours, while the same device operating at an average luminance of 100 cd m^{-2} (R = 28 μW) would last 70 hours. Thus, the lifetime can be increased at the expense of average luminance, and *vice versa*. It is therefore important, in general, to note the average radiant flux of a device when evaluating its lifetime.

The second regime observed in Fig. 6 corresponds to a dramatic decrease of E_{tot} by over an order of magnitude per volt. This would suggest that an additional quenching mechanism that is voltage dependent is activated for $V > 3.2$ V. To the best of our knowledge, this is the first time that this regime has been identified. One possible explanation for this accelerated degradation is multiple oxidation and subsequent decomposition of the $[Ru(bpy)_3]^{2+}(PF_6^-)_2$ complex due to excessive PF_6^- build-up at the anode.[76] In any event, it appears that an additional degradation mode is elicited at higher voltages.

Table 3 presents the average radiant flux and the total emitted energy for various iTMC devices. It is revealed that blending $[Ru(bpy)_3]^{2+}(PF_6^-)_2$ with PMMA increases $t_{1/5}$ by nearly two orders of magnitude. However, the average radiant flux of the PMMA blend is approximately a factor of 20 lower. As a result, E_{tot} differs only by a factor of 5. Similarly, the pristine $[Ir(ppy)_2(dtb\text{-}bpy)]^+(PF_6^-)$ device has a longer $t_{1/5}$ than the pristine $[Ru(bpy)_3]^{2+}(PF_6^-)_2$, but a lower E_{tot} due to a lower R. In these cases it is clear that an increased lifetime did not produce a similar increase in E_{tot}. Blending the $[Ir(ppy)_2(dtb\text{-}bpy)]^+(PF_6^-)$ complex with the ionic liquid 1-butyl-3-methylimidazolium $BMIM^+(PF_6^-)$ not only improves turn-on time, as noted below, but also lowers both $t_{1/5}$ and E_{tot}, and hence contributes to degradation.

As it is not possible to obtain these values precisely for every reported device, we will forego calculation for the following examples. However, we encourage the reader to consider these points when evaluating lifetime.

Humidity was found to significantly reduce $t_{1/2}$ of $[Ru(bpy)_3]^{2+}(ClO_4^-)_2$ devices by Pile *et al.*[43] A device exposed to 20% relative humidity (RH) exhibited a $t_{1/2}$ approximately a factor of 3 shorter than those held in a dry nitrogen environment, while those exposed to 63% RH experienced a drop in $t_{1/2}$ of over an order of magnitude. These observations were consistent with previous reports[21,27] where lifetimes of devices operated in the glove box were longer than those driven in air. Furthermore, bubbles were formed at higher concentrations near the cathode for those devices with higher RH exposure, attributed to reduction of the water and H_2 generation. It was postulated that the decrease in $t_{1/2}$ upon exposure to moisture was due to enhanced formation of $[Ru(bpy)_2(H_2O)_2]^{2+}$, a proposed luminescence quencher.[27] Oxygen was shown to have little influence on device lifetime.

Along these lines, Zhao *et al.*[50] investigated the effects of residual water and acetonitrile on $[Ru(bpy)_3]^{2+}(ClO_4^-)_2$ thin films and devices. Completed devices were baked in up to three steps, which involved: 1) baking in a conventional vacuum oven at 125 °C for 48 h; 2) holding under high vacuum (2×10^{-7} torr) for 24 h; and 3) baking at 143 °C for 12 h in an ultrahigh vacuum capable of achieving a base pressure of 6×10^{-10} torr. Devices subject to all three steps showed less decay in electroluminescence intensity over those that were only subject to the first two (9% over 2000 s as compared to 60%), though the initial intensity was approximately an order of magnitude lower. Upon baking films at 143 °C under ultra high vacuum and monitoring the presence of H_2O and MeCN by mass spectrometry, it was found that these species continued to desorb from the film even after 4 h of baking. It was concluded that films subject to conventional processing likely still retain a significant amount of water and solvent.

As observed previously for polymer-blended $[Ru(bpy)_3]^{2+}$ devices,[17,20] highly efficient devices were fabricated by Bolink *et al.*[51] by blending PMMA into $[Ru(dp\text{-}phen)_3]^{2+}$ films, where dp-phen is 4,7-diphenyl-1,10-phenanthroline. Lifetimes of up to $t_{1/2}$ = 115 h were obtained, an increase of nearly tenfold over the $[Ru(bpy)_3]^{2+}$ standards used in the experiment. The phenanthroline ligands were credited with improved hydrophobicity and increased resistance toward water-induced substitution reactions, leading to the higher stability. This same ligand also produced long lifetimes in Ir electroluminescent devices. The $t_{1/2}$ of an $[Ir(ppy)_2(dp\text{-}phen)]^+(PF_6^-)$ device was found by Bolink *et al.*[61] to be 65 h, the highest reported for a pristine Ir iTMC device to date. The stability was again attributed to the dp-phen ligand due to improved hydrophobicity and steric hindrance of overlap with ppy orbitals.

Two reports[56,63] have identified a quencher formed in $[Ru(bpy)_3]^{2+}(PF_6^-)_2$ devices, namely, the oxo-bridged dimer $[Ru(bpy)_2(H_2O)]_2O^{4+}(PF_6^-)_4$. First, Soltzberg *et al.*[56] used mass spectrometry to reveal that electrical driving of ITO/$[Ru(bpy)_3]^{2+}(PF_6^-)_2$/Au devices induces oxo-bridged dimerization. In particular, the $[Ru(bpy)_2(H_2O)]_2O^{4+}(PF_6^-)_4$ dimer was confirmed to form in the device by comparison of a run-device spectrum with that from the synthesized dimer. In contrast, the spectrum from a device subject to the same processing conditions but not electrically driven did not show any dimeric signature. It was demonstrated that this dimer serves as an effective quencher of device luminescence. Furthermore, *in situ* Raman spectroscopy of devices prepared and electrically driven in the same way revealed the formation of a characteristic series of peaks about 380 cm^{-1} associated with the Ru–O–Ru bond, thus confirming the result with a less invasive technique.

In a subsequent study, Slinker *et al.*[63] employed real-time, *in situ* Raman spectroscopy to reveal the sequential formation

Table 3 Lifetime, average radiant flux and total emitted energy data for 3 mm^2 ITO/iTMC/Au devices under 3 V applied bias

Active layer	$[Ru(bpy)_3]^{2+}(PF_6^-)_2$	$[Ru(bpy)_3]^{2+}(PF_6^-)_2$ w/PMMA[a]	$[Ir(ppy)_2(dtb\text{-}bpy)]^+(PF_6^-)$[b]	$[Ir(ppy)_2(dtb\text{-}bpy)]^+(PF_6^-)$ w/$BMIM^+PF_6^-$[b,c]
$t_{1/5}$/h	14	1090	26	9
R/W	2.3×10^{-5}	1.5×10^{-6}	2.9×10^{-6}	2.5×10^{-6}
E_{tot}/J	1.13	5.90	0.27	0.08

[a] 38% w/w PMMA [b] From ref. 41 [c] 0.25% v/v $BMIM^+(PF_6^-)$

of oxo-bridged dimers upon planar Au/$[Ru(bpy)_3]^{2+}(PF_6^-)_2$/Au device operation. The extent of the dimerization upon running the device for 1 hour was approximately 1% w/w. Fluorescence-microscopy images revealed that the device-film photoluminescence was effectively quenched. In an independent experiment, it was confirmed that oxo-bridged dimers such as $[Ru(bpy)_2(H_2O)]_2O^{4+}(PF_6^-)_4$ are effective photoluminescence quenchers, even at concentrations as low as 1% w/w. Thus, oxo-bridged dimerization occurred in the device to an extent that would account for luminescence quenching. Exposure of devices to oxygen led to significant, irreversible loss of radiant flux with time, supporting the assertion of luminescence quenching upon dimerization.

As iTMC devices can be fabricated with air-stable electrodes, suppression of these degradation reactions will lead to devices that are intrinsically resistant to degradation, potentially eliminating the need for encapsulation. Additional efforts are still needed to clarify specific degradation reaction pathways and prevent quencher formation in the device. The precise role of $[Ru(bpy)_2(H_2O)]^{2+}$ has yet to be clarified, as it could serve as a reaction intermediate to $[Ru(bpy)_2(H_2O)]_2O^{4+}(PF_6^-)_4$ dimer formation in $[Ru(bpy)_3]^{2+}(PF_6^-)_2$ devices. Furthermore, there is recent evidence of structural evolution in these films,[77] and the role of structure in device degradation has not been fully elucidated. Still, these recent results are promising steps in achieving long-lasting iTMC devices.

Turn-on time

In this section we discuss the influence of materials, device preparation and operation conditions on the turn-on time of iTMC-based devices. Turn-on time, defined as the time required to reach maximum emission under dc bias, has typically ranged from seconds to several hours.[5] However, for practical applications, turn-on times must be significantly reduced. Unfortunately, many schemes for improving turn-on time come at a cost to stability, as will be discussed below.

• Higher applied bias leads to faster turn-on times, but result in shorter lifetimes.[14,24] To achieve this faster turn-on but avoid the higher degradation rate, Handy *et al.*[14] used a pulsed-biasing scheme—a short pulse at a higher voltage was used to turn the device on, followed by a lower voltage that was used to drive the device for extended periods. This technique has received recent attention.[54,55,60]

• Reducing the thickness of the iTMC layer reduces the turn-on time, but leads to a decrease in the efficiency due to exciton quenching at the electrodes.[28]

• Complex, bulky ligands tend to lead to longer turn-on times.[14,29]

• Smaller counterions such as BF_4^- or ClO_4^- yield faster turn-on times than PF_6^-, but also negatively impact lifetime.[16,20]

• Addition of an electrolyte to the iTMC layer has improved lifetimes, as has including additional ions.[13,25] However, these approaches diminish lifetime as well.

• Devices run in air show shorter turn-on times than those run in a nitrogen environment, but this also leads to faster decay of radiant flux.[21,27]

According to the electrodynamic model,[66,67] device turn-on time is determined by the speed at which counterion redistribution near the electrodes takes place. Increased concentration and/or mobility of counterions leads to a shorter amount of time for ionic redistribution to occur near the electrodes, and the devices turn on faster. Thus, the focus has shifted to factors influencing the ionic conductivity, which has led to improved understanding and control of turn-on time.

Along these lines, ionic liquids have been added to the iTMC layer to reduce turn-on time.[40–41,52] Inclusion of the ionic liquid enhanced the ionic conductivity by increasing the ionic mobility and density of mobile ions. By introducing the ionic liquid 1-butyl-3-methylimidazolium hexafluorophosphate $BMIM^+(PF_6^-)$ into devices based on $[Ir(F\text{-}mppy)_2(dtb\text{-}bpy)]^+(PF_6^-)$, Slinker *et al.*[40] achieved a reduction of turn-on time from 4 h to 40 min. In a thorough study involving this same ionic liquid, Parker *et al.*[41] likewise demonstrated improved turn-on times of $[Ir(ppy)_2(dtb\text{-}bpy)]^+(PF_6^-)$ without altering device efficiency significantly. For a blend with 0.25% v/v $BMIM^+(PF_6^-)$, the turn-on time was reduced from approximately 5 h to 40 min. The lifetime was reduced by a factor of 3 at this concentration. Although the ultimate turn-on time in these devices is still long, the order-of-magnitude decrease was substantial.

By using a $[Ru(dtb\text{-}bpy)_3]^{2+}(PF_6^-)_2$ complex with $BMIM^+(PF_6^-)$, Slinker *et al.*[52] achieved turn-on times between 1–10 ms and ac operation at 60 Hz. The dtb-bpy ligands were reported to give the best phase compatibility with $BMIM^+(PF_6^-)$ among a series of Ru compounds. This high compatibility enabled the rapid turn-on time necessary for 60 Hz operation, as shown in Fig. 7. Emission, though asymmetric, occurred in both forward and reverse bias sweeps and appeared constant to the eye. Together with a cascaded device architecture to scale-up voltage, operation of ''plug and

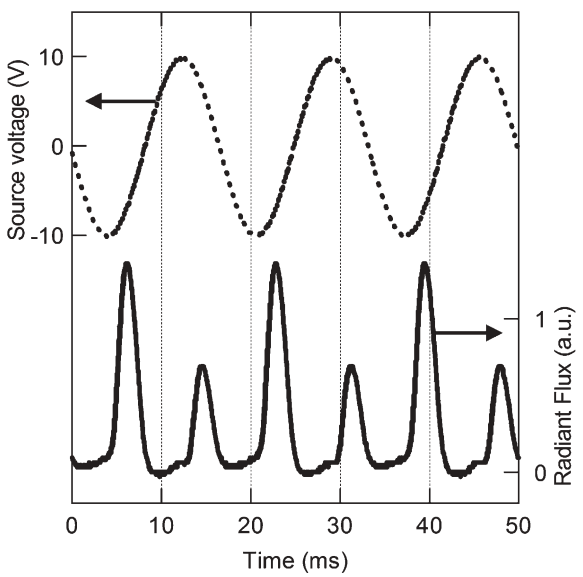

Fig. 7 (From Fig. 2, Ref. 52) Source voltage (dotted lines) and radiant flux (solid lines) *versus* time for a single ITO/$[Ru(dtb\text{-}bpy)_3]^{2+}(PF_6^-)_2$–$BMIM^+(PF_6^-)$/Au device operating at 60 Hz. Reproduced with permission from *J. Appl. Phys.*, 2006, **99**, 074502. Copyright 2006, American Institute of Physics.

play'' organic LEC lighting panel was achieved, sourced directly from a standard US outlet (110–120 V rms, 60 Hz).

Environmental effects during both device operation and preparation have been shown to influence turn-on time. Two reports have delineated the effects of moisture and residual solvent on device turn-on time. Pile and Bard[43] investigated the effects of moisture on $[Ru(bpy)_3]^{2+}(ClO_4^-)$ thin films and devices. Devices were tested in a closed chamber and exposed to humidity levels between 0 and 63% relative humidity (RH). Turn-on time was observed to follow an inverse relationship with RH, with exposure levels over 25% RH leading to tenfold or greater reduction. Zhao *et al.*[50] showed that the operation of $[Ru(bpy)_3]^{2+}(ClO_4^-)$ devices is strongly influenced by residual H_2O and solvent (acetonitrile) in the film remaining from the solution deposition. In short, films dried under higher vacuum showed longer turn-on times, higher turn-on voltages, and greater stability. Such results can be understood by the fact that residual water and solvent play a large role in the mobility of the counter ions.

Further work is still necessary to improve turn-on time and understand the apparent trade-off between turn-on time and lifetime. For devices involving fast ac operation, improvements in turn-on time and lifetime should be directly correlated as improved ionic conductivity will reduce the operational voltage. For dc operation, improving the turn-on time–lifetime trade-off will likely involve control over the magnitude of the space charge accumulating near the electrodes so as to avoid electrochemical degradation reactions.

Outlook

Ionic transition metal complexes offer unique opportunities for devices with novel architectures. Some of these architectures utilize the ability of iTMCs to inject electrons and holes from the same electrode. In others, ions give rise to electric fields that control electronic current flow. From panels for large-area illumination to nano-scale emitters, the future for potential applications of iTMC devices looks promising.

Bernards *et al.*[38] demonstrated ITO/$[Ru(dtb\text{-}bpy)_3]^{2+}(PF_6^-)_2$/Au devices with laminated top contacts, important for roll-to-roll processing of devices. These devices were fabricated by evaporating the Au electrode onto a polydimethylsiloxane (PDMS) stamp, followed by soft contact lamination of this stamp onto an ITO/$[Ru(dtb\text{-}bpy)_3]^{2+}(PF_6^-)_2$ substrate. Devices with laminated top contacts showed equivalent performance to those fabricated with evaporated top contacts, indicating high quality lamination. Furthermore, these devices showed no rectification, indicating that the resulting contact was ohmic and that the lamination process caused no damage to the ruthenium complex.

Two recent efforts with iTMC devices have important implications for lighting. Bernards *et al.*[39] fabricated a cascaded panel exhibiting scalability and fault tolerance to shorts. This panel was fabricated with Au top contacts and ITO bottom contacts with an $[Ru(dtb\text{-}bpy)_3]^{2+}(PF_6^-)_2$ active layer. The electrodes were patterned such that the anode of one device served as the cathode of the next. Panels with $N = 1$ to 4 devices were prepared, and a bias of $3N$ was applied across each panel. The current was independent of N, while the radiant flux and EQE each scaled with N. An $N = 4$ panel was shown to continue operating even with a shorted device, demonstrating intrinsic fault tolerance.

Putting this technique to practice, Slinker *et al.*[52] demonstrated lighting panels from iTMC devices with direct outlet operation at 120 V rms, 60 Hz. Millisecond turn-on times were achieved by introducing small quantities of the ionic liquid $BMIM^+(PF_6^-)$ in the iTMC film. The high voltage was supported by fabricating cascaded device panels, thus distributing the voltage over several devices. Outlet operation of such a panel is shown in Fig. 8.

Recently, Bernards *et al.*[57] exploited the ionic nature of iTMCs to fabricate a novel light-emitting device employing a solid-state ionic PN junction. A bilayer device of the structure ITO/$DPAS^-Na^+$/$[Ru(bpy)_3]^{2+}(PF_6^-)_2$/Au was formed by soft-contact lamination, where $DPAS^-Na^+$ denotes sodium 9,10-diphenylanthracene-2-sulfonate. In this configuration, the Na^+ from the $DPAS^-$ layer diffused into the $[Ru(bpy)_3]^{2+}$ layer, and the PF_6^- counterions diffused from the iTMC into the $DPAS^-$ material. This created excess negative ionic charge in the $DPAS^-$ layer, and positive ionic-space charge on the $[Ru(bpy)_3]^{2+}$ side, thus forming an ionic PN junction, analogous to an electronic pn junction formed in conventional semiconductors. Interestingly, though single-layer light-emitting devices based on either $[Ru(bpy)_3]^{2+}(PF_6^-)_2$ or $DPAS^-Na^+$ showed no rectification in current or radiant flux, the bilayer device exhibited significant rectification in both. This was believed to be caused by an ionic PN junction formed in the center of the device, analogous to a traditional pn junction. Similarly, a photovoltaic response was observed from the bilayer device, though the devices based on the single-layer components did not. This work shows that mobile ionic charge can dictate the flow of electronic current in solid-state electronic devices.

Transitioning from macroscale to microscale light emitters, electroluminescent nanofibers from iTMC–PEO mixtures have been recently reported by Moran-Mirabal *et al.*[64] These fibers were electrospun onto Au-interdigitated electrodes. The electroluminescence along the fiber's radius was limited to the fiber dimensions, while emission along the axis of the fiber occupied only a small fraction of the inter-electrode

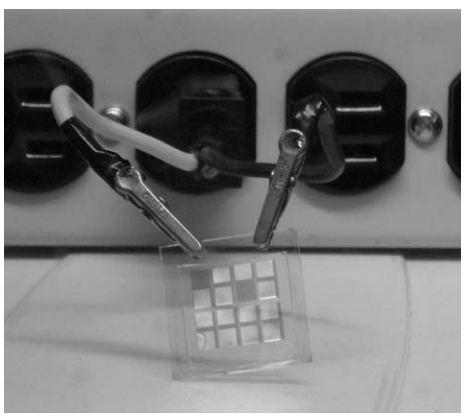

Fig. 8 (From Fig. 4b, Ref. 52) Cascaded panel operating directly from a standard US outlet. Reproduced with permission from *J. Appl. Phys.*, 2006, **99**, 074502. Copyright 2006, American Institute of Physics.

spacing. The full width at half maximum (FWHM) emissive areas were as small as 240 by 325 nm along the radius and axis, respectively, indicating that these devices served as sub-wavelength point sources (λ_{max} = 600 nm). The ease of fabrication and the precision of the electroluminescence make these devices attractive candidates for spectroscopic, sensing, and lab-on-a-chip applications where localized emission is desired.

Acknowledgements

We would like to thank the NSF, NYSTAR, the Cornell Nanofabrication Facility and the Cornell High Energy Synchrotron Source. JDS was supported by an NSF Graduate Research Fellowship. The authors would like to thank Dan Bernards and Matt Lloyd for helpful comments.

References

1 G. Malliaras and R. Friend, *Phys. Today*, 2005, **14**(5), 53–58.
2 A. Bergh, G. Craford, A. Duggal and R. Haitz, *Phys. Today*, 2001, **54**(12), 42–47.
3 E. Holder, B. M. W. Langeveld and U. S. Schubert, *Adv. Mater.*, 2005, **17**, 1109–1121.
4 Y. R. Sun, N. C. Giebink, H. Kanno, B. W. Ma, M. E. Thompson and S. R. Forrest, *Nature*, 2006, **440**, 908–912.
5 J. Slinker, D. Bernards, P. L. Houston, H. D. Abruña, S. Bernhard and G. G. Malliaras, *Chem. Commun.*, 2003, 2392–2399.
6 J. K. Lee, D. S. Yoo, E. S. Handy and M. F. Rubner, *Appl. Phys. Lett.*, 1996, **69**, 1686–1688.
7 K. M. Maness, R. H. Terrill, T. J. Meyer, R. W. Murray and R. M. Wightman, *J. Am. Chem. Soc.*, 1996, **118**, 10609–10616.
8 K. M. Maness, H. Masui, R. M. Wightman and R. W. Murray, *J. Am. Chem. Soc.*, 1997, **119**, 3987–3993.
9 J. K. Lee, D. S. Yoo and M. F. Rubner, *Chem. Mater.*, 1997, **9**, 1710–1712.
10 C. M. Elliott, F. Pichot, C. J. Bloom and L. S. Rider, *J. Am. Chem. Soc.*, 1998, **120**, 6781–6784.
11 A. P. Wu, J. K. Lee and M. F. Rubner, *Thin Solid Films*, 1998, **329**, 663–667.
12 X. Gong, P. K. Ng and W. K. Chan, *Adv. Mater.*, 1998, **10**, 1337–1340.
13 C. H. Lyons, E. D. Abbas, J. K. Lee and M. F. Rubner, *J. Am. Chem. Soc.*, 1998, **120**, 12100–12107.
14 E. S. Handy, A. J. Pal and M. F. Rubner, *J. Am. Chem. Soc.*, 1999, **121**, 3525–3528.
15 A. P. Wu, D. S. Yoo, J. K. Lee and M. F. Rubner, *J. Am. Chem. Soc.*, 1999, **121**, 4883–4891.
16 F. G. Gao and A. J. Bard, *J. Am. Chem. Soc.*, 2000, **122**, 7426–7427.
17 H. Rudmann and M. F. Rubner, *J. Appl. Phys.*, 2001, **90**, 4338–4345.
18 S. Bernhard, X. Gao, G. G. Malliaras and H. D. Abruña, *Adv. Mater.*, 2002, **14**, 433–436.
19 C. Y. Liu and A. J. Bard, *J. Am. Chem. Soc.*, 2002, **124**, 4190–4191.
20 H. Rudmann, S. Shimada and M. F. Rubner, *J. Am. Chem. Soc.*, 2002, **124**, 4918–4921.
21 M. Buda, G. Kalyuzhny and A. J. Bard, *J. Am. Chem. Soc.*, 2002, **124**, 6090–6098.
22 H. Rudmann, S. Shimada, M. F. Rubner, D. W. Oblas and J. E. Whitten, *J. Appl. Phys.*, 2002, **92**, 1576–1581.
23 F. G. Gao and A. J. Bard, *Chem. Mater.*, 2002, **14**, 3465–3470.
24 S. Bernhard, J. A. Barron, P. L. Houston, H. D. Abruña, J. L. Ruglovksy, X. Gao and G. G. Malliaras, *J. Am. Chem. Soc.*, 2002, **124**, 13624–13628.
25 J.-C. Leprêtre, A. Deronzier and O. Stéphan, *Synth. Met.*, 2002, **131**, 175–183.
26 J. D. Slinker, A. A. Gorodetsky, M. S. Lowry, J. Wang, S. Parker, R. Rohl, S. Bernhard and G. G. Malliaras, *J. Am. Chem. Soc.*, 2004, **126**, 2763–2767.
27 G. Kalyuzhny, M. Buda, J. McNeill, P. Barbara and A. J. Bard, *J. Am. Chem. Soc.*, 2003, **125**, 6272–6283.
28 K. W. Lee, J. Slinker, A. A. Gorodetsky, S. Flores-Torres, H. D. Abruña, P. L. Houston and G. G. Malliaras, *Phys. Chem. Chem. Phys.*, 2003, **5**, 2706–2709.
29 J. A. Barron, S. Bernhard, P. L. Houston, H. D. Abruña, J. Ruglovsky and G. G. Malliaras, *J. Phys. Chem.*, 2003, **107**, 8130–8133.
30 F.-R. F. Fan and A. J. Bard, *J. Phys. Chem. B*, 2003, **107**, 1781–1787.
31 H. Rudmann, S. Shimada and M. F. Rubner, *J. Appl. Phys.*, 2003, **94**, 115–122.
32 W. Y. Ng, X. Gong and W. K. Chan, *Chem. Mater.*, 1999, **11**, 1165–1170.
33 W. K. Chan, P. K. Ng, X. Gong and S. Hou, *Appl. Phys. Lett.*, 1999, **75**, 3920–3922.
34 X. Gong, P. K. Ng and W. K. Chan, *J. Nanosci. Nanotechnol.*, 2002, **2**(2), 151–154.
35 C.-Y. Liu and A. J. Bard, *Appl. Phys. Lett.*, 2003, **83**, 5431–5433.
36 A. A. Gorodetsky, S. Parker, J. D. Slinker, D. A. Bernards, M. H. Wong, G. G. Malliaras, S. Flores-Torres and H. D. Abruña, *Appl. Phys. Lett.*, 2004, **84**, 807–809.
37 J. D. Slinker, G. G. Malliaras, S. Flores-Torres, H. D. Abruña, W. Chunwachirasiri and M. J. Winokur, *J. Appl. Phys.*, 2004, **95**, 4381–4384.
38 D. A. Bernards, T. Biegala, Z. A. Samuels, J. D. Slinker, G. G. Malliaras, S. Flores-Torres, H. D. Abruña and J. A. Rogers, *Appl. Phys. Lett.*, 2004, **84**, 3675–3677.
39 D. A. Bernards, J. D. Slinker, G. G. Malliaras, S. Flores-Torres and H. D. Abruña, *Appl. Phys. Lett.*, 2004, **84**, 4980–4982.
40 J. D. Slinker, C. Y. Koh, G. G. Malliaras, M. S. Lowry and S. Bernhard, *Appl. Phys. Lett.*, 2005, **86**, 173506.
41 S. T. Parker, J. D. Slinker, M. S. Lowry, M. P. Cox, S. Bernhard and G. G. Malliaras, *Chem. Mater.*, 2005, **17**, 3187–3190.
42 C.-Y. Liu and A. J. Bard, *Appl. Phys. Lett.*, 2005, **87**, 061110.
43 D. L. Pile and A. J. Bard, *Chem. Mater.*, 2005, **17**, 4212–4217.
44 H. J. Bolink, L. Cappelli, E. Coronado and P. Gaviña, *Inorg. Chem.*, 2005, **44**, 5966–5968.
45 C. Zhen, Y. Chuai, C. Lao, L. Huang, D. Zou, D. N. Lee and B. H. Kim, *Appl. Phys. Lett.*, 2005, **87**, 093508.
46 M. S. Lowry, J. I. Goldsmith, J. D. Slinker, R. Rohl, R. A. Pascal, Jr., G. G. Malliaras and S. Bernhard, *Chem. Mater.*, 2005, **17**, 5712–5719.
47 A. B. Tamayo, S. Garon, T. Sajoto, P. I. Djurovich, I. M. Tsyba, R. Bau and M. E. Thompson, *Inorg. Chem.*, 2005, **44**, 8723–8732.
48 A. R. Hosseini, C. Y. Koh, J. D. Slinker, S. Flores-Torres, H. D. Abruña and G. G. Malliaras, *Chem. Mater.*, 2005, **17**, 6114–6116.
49 Y.-M. Wang, F. Teng, Y.-B. Hou, Z. Xu, Y.-S. Wang and W.-F. Fu, *Appl. Phys. Lett.*, 2005, **87**, 233512.
50 W. Zhao, C.-Y. Liu, Q. Wang, J. M. White and A. J. Bard, *Chem. Mater.*, 2005, **17**, 6403–6406.
51 H. J. Bolink, L. Cappelli, E. Coronado, M. Grätzel and M. K. Nazeeruddin, *J. Am. Chem. Soc.*, 2006, **128**, 46–47.
52 J. D. Slinker, J. Rivnay, J. A. DeFranco, D. A. Bernards, A. A. Gorodetsky, S. T. Parker, M. P. Cox, R. Rohl, G. G. Malliaras, S. Flores-Torres and H. D. Abruña, *J. Appl. Phys.*, 2006, **99**, 074502.
53 H. J. Bolink, L. Cappelli, E. Coronado, A. Parham and P. Stössel, *Chem. Mater.*, 2006, **18**, 2778–2780.
54 N. Armaroli, G. Accorsi, M. Holler, O. Moudam, J.-F. Nierengarten, Z. Zhou, R. T. Wegh and R. Welter, *Adv. Mater.*, 2006, **18**, 1313–1316.
55 Q. Zhang, Q. Zhou, Y. Cheng, L. Wang, D. Ma, X. Jing and F. Wang, *Adv. Funct. Mater.*, 2006, **16**, 1203–1208.
56 L. J. Soltzberg, J. D. Slinker, S. Flores-Torres, D. A. Bernards, G. G. Malliaras, H. D. Abruña, J.-S. Kim, R. H. Friend, M. D. Kaplan and V. Goldberg, *J. Am. Chem. Soc.*, 2006, **128**, 7761–7764.
57 D. A. Bernards, S. Flores-Torres, H. D. Abruña and G. G. Malliaras, *Science*, 2006, **313**, 1416–1419.
58 F. Wang, P. Wang, X. Fan, X. Dang, C. Zhen, D. Zou, E. H. Kim, D. N. Lee and B. H. Kim, *Appl. Phys. Lett.*, 2006, **89**, 183519.

59 S. Wang, X. Li, S. Xun, X. Wan and Z. Y. Wang, *Macromolecules*, 2006, **39**, 7502–7507.
60 M. K. Nazeeruddin, R. T. Wegh, Z. Zhou, C. Klein, Q. Wang, F. De Angelis, S. Fantacci and M. Grätzel, *Inorg. Chem.*, 2006, **45**, 9245–9250.
61 H. J. Bolink, L. Cappelli, E. Coronado, M. Grätzel, E. Ortí, R. D. Costa, P. M. Viruela and M. K. Nazeeruddin, *J. Am. Chem. Soc.*, 2006, **128**, 14786–14787.
62 H.-C. Su, C.-C. Wu, F.-C. Fang and K.-T. Wong, *Appl. Phys. Lett.*, 2006, **89**, 261118.
63 J. D. Slinker, J.-S. Kim, S. Flores-Torres, J. H. Delcamp, H. D. Abruña, R. H. Friend and G. G. Malliaras, *J. Mater. Chem.*, 2007, **17**, 76–81.
64 J. Moran-Mirabal, J. D. Slinker, J. A. DeFranco, S. S. Verbridge, R. Ilic, S. Flores-Torres, H. Abruña, G. G. Malliaras and H. G. Craighead, *Nano Lett.*, 2007, **7**, 458–463.
65 H.-C. Su, F.-C. Fang, T.-Y. Hwu, H.-H. Hsieh, H.-F. Chen, G.-H. Lee, S.-M. Peng, K.-T. Wong and C.-C. Wu, *Adv. Funct. Mater.*, 2007, **17**, 1019–1027.
66 J. C. deMello, N. Tessler, S. C. Graham and R. H. Friend, *Phys. Rev. B*, 1998, **57**, 12951–12963.
67 J. C. deMello, *Phys. Rev. B*, 2002, **66**, 235210.
68 Q. B. Pei, G. Yu, C. Zhang, Y. Yang and A. J. Heeger, *Science*, 1995, **269**, 1086–1088.
69 D. M. Roundhill, *Photochemistry and Photophysics of Metal Complexes*, Plenum, New York, 1994.
70 K. Kalyanasundaram, *Photochemistry of Polypyridine and Porphyrin Complexes*, Academic Press, London, 1992.
71 H. Yersin, *Top. Curr. Chem.*, 2004, **241**, 1–26.
72 B. J. Coe and N. R. M. Curati, *Comments Inorg. Chem.*, 2004, **25**, 147–184.
73 H. Xia, C. Zhang, X. Liu, S. Qiu, P. Lu, F. Shen, J. Zhang and Y. Ma, *J. Phys. Chem. B*, 2004, **108**, 3185–3190.
74 E. A. Plummer, A. van Dijken, H. W. Hoffstraat, L. DeCola and K. Brunner, *Adv. Funct. Mater.*, 2005, **15**, 281–289.
75 J.-P. Sauvage, J.-P. Collin, J.-C. Chambron, S. Guillerez, C. Coudret, V. Balzani, F. Barigelletti, L. De Cola and L. Flamigni, *Chem. Rev.*, 1994, **94**, 993–1019.
76 E. Garcia, J. Kwak and A. J. Bard, *Inorg. Chem.*, 1988, **27**, 4377–4382.
77 D. R. Blasini, J. Rivnay, D.-M. Smilgies, J. D. Slinker, S. Flores-Torres, H. D. Abruña and G. G. Malliaras, *J. Mater. Chem.*, 2007, **17**, 1458–1461.

